# Scanning Tunnel Microscope

Laboratory Report by

**Annika Meyer, Isabell Suchy**
**and Sara Buhigas Torres**

Tutorin: Bharti Mahendru

**Fortgeschrittenenpraktikum, SoSe 2025**

Freie Universität Berlin
Department of Physics

# 1 Introduction

Scanning Tunnel Microscopy allows the examination of surface structures of conductive and semi-conductive materials on an atomic level. The aim of the following experiments is to develop familiarity with using a Scanning Tunnel Microscope (STM), the theory behind it and to explore the effects of some of the microscope's settings. Additionally, the surface structure of graphite will be recorded and possible visible atomic structures analyzed. The objective then is to determine the lattice constant and the distance between the layers of the graphite sample. [10]

# 2 Theoretical Basis

## 2.1 Quantum tunneling

Quantum tunneling describes the process of a particle being able to cross a potential energy barrier even though it does not have enough energy to cross "above" the barrier when looking at the problem using classical mechanics, thus the particle "tunnels" through the barrier, due to its wave nature. Within the barrier the wave function of the particle decreases exponentially, the further it has traveled within the barrier (see Fig. 1). [17]

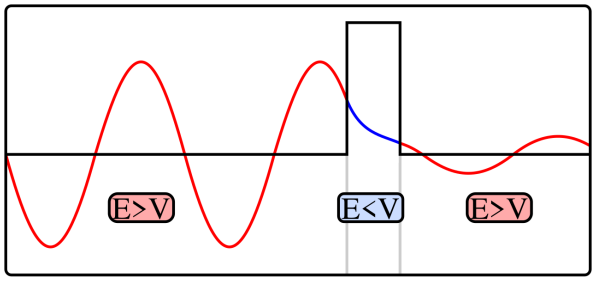


Figure 1: Schematic description of quantum tunneling along a 2-dimensional potential barrier. The wave function decreases exponentially within the barrier the further the particle travels, and sometimes still exists beyond the barrier. [16]

Within the STM the distance between the tip and the surface represents such a potential energy barrier, with the wave function of the electrons decreasing exponentially above the boundary of the surface, as described by equation 2.6. If the gap is small enough (<10 Å), the electrons are able to tunnel to the tip. A bias voltage is applied to ensure that tunneling is directional from the sample to the tip and not the other way around. The tunneling current $I_t$ created is dependent on the size of the gap s:

$$I_t \approx V_t \cdot e^{-c \cdot \sqrt{\Phi} \cdot s} \tag{1}$$

$V_t$ describes the differential potential between tip and surface, $c \approx 1.02^{-1} eV^{-\frac{1}{2}}$, $\Phi$ is the work function in eV, and s is the distance between surface and tip in Å. [10]

## 2.2 Piezo-electric effect

The very precise movements of the STM tip are achieved through the use of piezo-electric crystals. When piezo-electric crystals expand or contract they induce an electric field, this is known as the piezo electric effect. The effect occurs when the unit lattice of the crystal does not have a center of inversion, thus when the crystal is deformed (stress or strains), microscopic dipoles form within it, these can be summed up and create a measurable potential difference. Within the STM set-up the inverse piezo-electric effect is utilized, where an electric field leads to a mechanical force. The crystals allow very precise movements for the STM tip, but limit the size of the scanned surface, in this case to $20\mu m \times 20\mu m$. [18, 10]

## 2.3 Scanning tunneling microscope

The STM consists of a very sharp conductive tip, which drives over the surface of the material. Due to the short distance between the tip and the surface, electrons are able to quantum tunnel between them. The applied voltage difference between the tip and the surface (10mV-1V) directs in which direction the electrons go (quantum tunnel) more frequently. As the electrons overcome the potential energy barrier, i.e. the gap between the tip and the surface, a tunneling current $I_t$ is measured at the tip. This measured current has an exponential dependency to the size of the gap between surface and tip.
There are two main modes of measurement of the tunneling current: constant current and constant height mode. In the constant current mode $I_t$ is held constant through continuous height adjustments of the tip, creating a near constant distance between the surface and the tip. With the constant height mode on the other hand, the tip is not varied along the z-Axis, creating a high variability of $I_t$ but also allowing for faster scanning. This mode can however only scan materials with atomically flat surfaces, while the constant current mode has a higher variability of materials it can asses. The difference between the two modes is further illustrated in fig. 2. [19, 10]

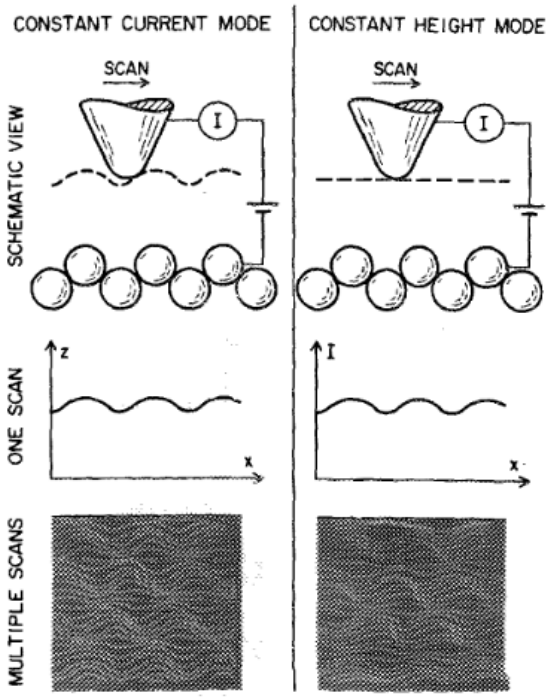


Figure 2: Different scanning modes of the STM. In the constant current mode the height of the STM tip is adjusted depending on the surface structure, allowing for a large range of height variability but longer scan times, while in the constant height mode the height of the STM tip is kept constant, requiring atomically flat surfaces but shorter scan times. [19 p.2]

### 2.4 Tunneling spectroscopy

While the scanning tunneling microscope (STM) is used to determine the surface structure in the form of images with atomic resolution, the scanning tunneling spectroscopy (STS) is a method which uses the STM to provide information about the density of electrons in a sample, which offers more detailed information about the structure of the surface. This is done by using the probe of the STM in a spectroscopic mode, which means making use of the voltage dependency. In this mode the probe is able to collect information about the electronic states of the surface within a few eV on either side of the Fermi level.13

### 2.5 Feedback and control circuits

To keep the tunnel current $I_t$ constant, the height of the tip is constantly readjusted via a electronic measurement and control system. The probe uses piezo electric positioning elements for the X and Y signal. The signals are received by the circuit, which then feeds a Z-signal back to the piezo element of the probe to adjust its height.1
The control system used is a Proportional Integral Derivative (PID) controller, which is a part of the feedback-loop mechanism. The PID constantly compares the output current with the desired input current and calculates their proportional, integral and derivative values. The proportional component is responsible for a fast reaction of the output to achieve the desired input current. The integral component accumulates the measured errors over time and corrects

constant errors, while the differential component calculates how the measured value will evolve over time and steers against the P and I value to prevent overshooting.14

## 2.6 Spatial and electronic structure of solids

The arrangement and organization of atoms or molecules in a solid material is described by their spatial structure. It can be categorized by different properties such as lattice structure, the corresponding basis and translation vectors and the resulting symmetries.
A solid material can have an amorphous or a crystalline structure and while the arrangement of atoms in amorphous solids is largely irregular, crystalline solids have a well-defined lattice structure with a three-dimensional periodic arrangement. The smallest repeating unit of a crystal lattice that, when replicated throughout space, generates the entire crystal structure, is called a unit cell.
One of the most common crystalline structured minerals is graphite. It is a widely distributed allotrope of carbon and has a stable hexagonal crystal structure. Graphite consists of layers of hexagonally arranged carbon atoms connected by covalent bonds. The carbon atoms are in $sp^2$-hybridized states. To hybridize, the orbitals of a single carbon atom first rearrange as shown in figure 3 which in this case is the energetically more favorable way.

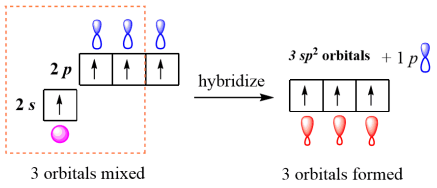


Figure 3: Scheme of the $sp^2$-hybridization of carbon atoms. 3

The hybridized orbitals then can overlap with the $sp^2$ hybrid orbitals of three neighboring carbon atoms. The fact that one of the $p$-orbitals is now the only non-bonded component is the reason for which graphite is electrically conductive. The electron of this orbital is non-localized and therefore allows conductivity within the layers and the usage of scanning tunneling microscopy.

The layers are stacked in parallel planes held together by van-der-Waals forces. As shown in figure 4, two carbon atoms in the same layer have a distance of $0,14$nm and the layers itself have a distance of $0,34$nm. 5

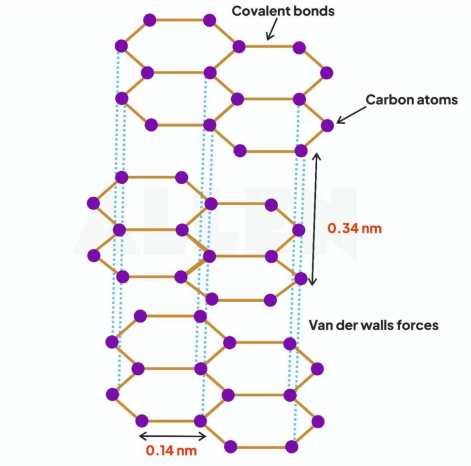


Figure 4: Spatial structure of graphite. 6

The layering occurs in ABAB stacking, meaning that every second layer is congruent which is shown in figure 5.

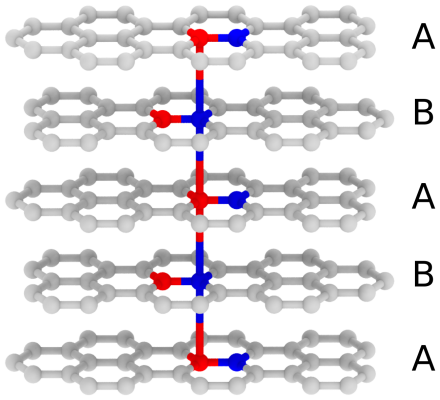


Figure 5: ABAB stacking of graphene layers. 8

A certain type of graphite is the Highly oriented pyrolytic graphite (HOPG) which is a form of synthetic graphite. The angular spread in the stacking of the graphene layers and crystallites is less than 2 degree, which makes HOPG extremely high in purity and ordered and therefore ideal for research. 7

The symmetry of crystalline solids is disturbed by the surface where the periodicity breaks. The existence of an interface results in a potential threshold and therefore provides boundary conditions for the propagation of the wave function of the electrons. The boundary conditions cause the amplitude of the wave function to drop exponentially when leaving the solid. 10 This is described by

$$\Psi = \Psi_0 \cdot e^{-\chi z}, \tag{2}$$

where $\chi$ represents the damping constant. It varies with the binding energy of the state $\Psi$. If this energy is near the Fermi-Energy, which is the highest energy that a fermion such as an electron in a many-particle system of similar fermions can have when the system is in the ground state, then $\chi$ is smallest. 9 As a result, the amplitude of the wave function drops slower and the wave function is visible further out of the solid. The further out the wave function reaches, the brighter it is detected by the probe head. So by visualizing the electron density distribution at the surface, scanning tunneling microscopy allows resolution on an atomic scale. 10

## 2.7 Fourier transform

The operation of Fourier transformation makes the transformation of data from the time or spatial domain to the frequency domain possible. Within scanning tunneling microscopy, 2D-Fourier transformation is used to analyze and interpret the measured data.
The image received through scanning tunneling microscopy is in the spatial domain. It can already show the periodic pattern of the sample. However by transforming the image to the frequency domain, the image is transformed into its reciprocal space. The result shows peaks whose distance from the origin corresponds exactly to the reciprocal lattice constant and precise conclusions about the real lattice constant become possible.
In addition symmetries appear as a geometric pattern of peaks in the frequency domain, which is often easier to identify than the pattern in the spatial domain. This is shown in figure 12.
Furthermore, Fourier transformation makes it possible to reduce perturbation of the data, such as noise or other defects, by filtering out specific frequency components. Now the inverse transformation back to the spatial domain provides a cleaned image of the sample. 11

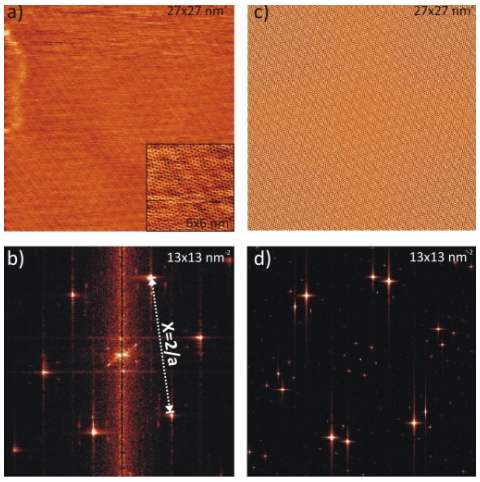


Figure 6: STM images in spatial (a,c) and frequency (b,d) domain. 12

# 3 Experimental Setup

The STM provided for the experiments is based on a proprietary set-up of the AG Franke which can operate in atmospheric conditions.To control the X- and Y- piezo elements there is a Digital/Analog converter as well as one for the measuring of the Z-voltage created by the feedback-control loop. These are used via the PC with the freeware WSxM supplied by Nanotec 1.

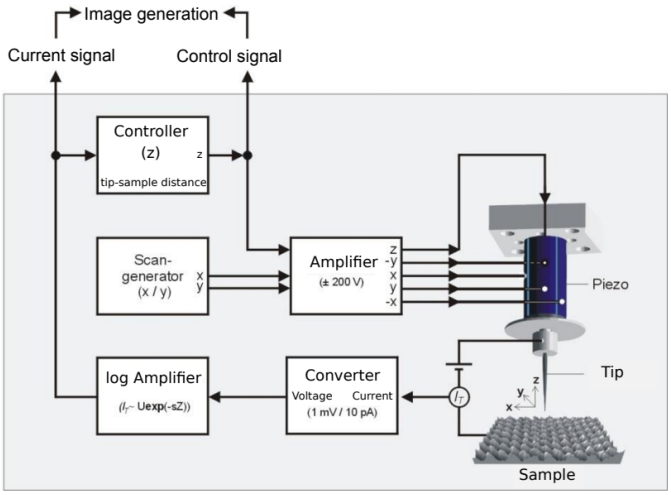


Figure 7: Block diagram of the STM 15

# 4 Step height determination

To determine the distance between different layers of graphite, areas with several visible steps were found with the STM and scanned. Using the program Gwyddion these STM Images were analyzed.[20]
The image was filtered using *"Reihenangleichen mittels verschiedener Methoden"* and *"Horizontale Fehlerzeilen korrigieren"*, allowing for a better overview of the image. Changing the color scale also achieved this. Then areas with one to two step edges were found and cropped. Three points were used to mark one plane (*"Daten mittels Ebene druch drei Punkte nivellieren"*) and further filter the data. If necessary the image was cropped again to remove outliers and noise. Next line profiles of the data were made and the heights between the steps determined using a built-in measurement tool. An example of such a line profile can be seen in fig. 8.

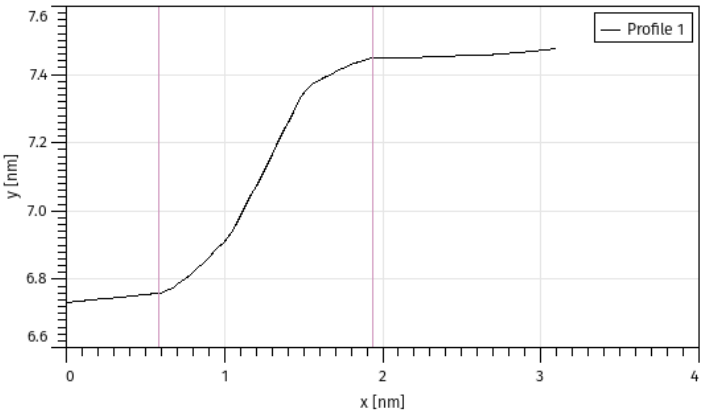


Figure 8: An example of a depth profile measured of graphite which shows one step, with the depth represented on the y-axis and the length on the x-axis. The purple vertical lines are manually placed to measure the step-height, there is some height variation visible within the graph especially towards the beginning and end where a continual height gradient is visible.

The heights of the different line profiles were then ordered by size and represented graphically in fig. 9. Blue horizontal lines represent the literature values of the different graphite layers with a distance of $\Delta d = 0,335nm$. [10]

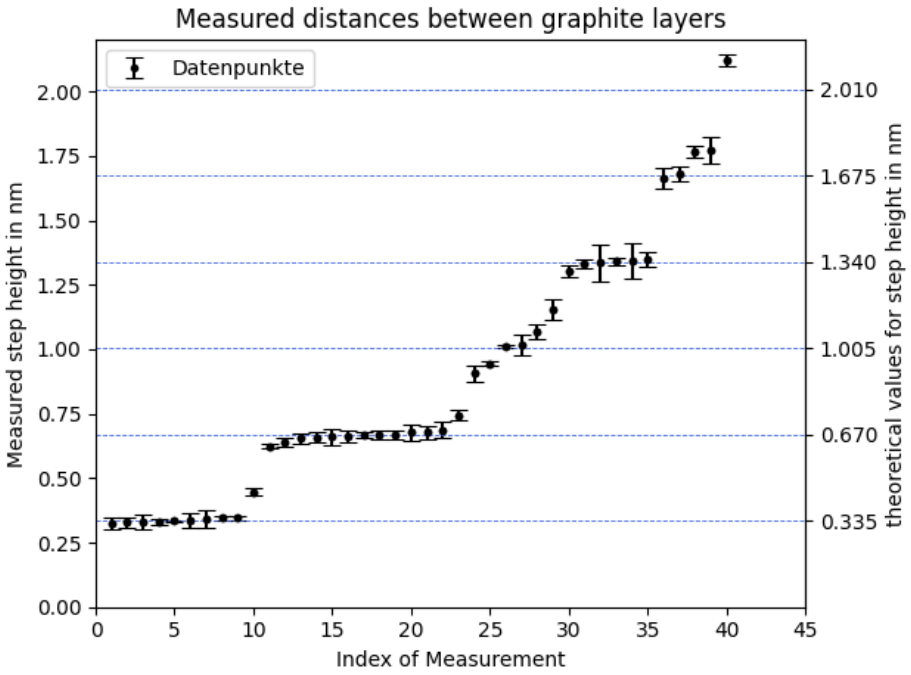


Figure 9: Graphical representation of the measured heights between graphite layers sorted by size. The blue dotted lines with description on the secondary y-axis show the values for the graphite layers found in literature.

The error within the data varied a lot. It was decided to measure the variation within the plane of each step height as described in fig. 8, which delivered small errors with some exceptions as can be seen in fig 9. The error within the data is relatively large. Due to noise that couldn't be filtered out further, the line graphs had some variation within them.
Overall the measurements correspond to the literary values, especially in the measurements for one or two graphite layers. However, at three or four graphite layers some variation can be seen with several measurements directly between the expected values of the two layers. Additionally, the expected value for five graphite layers was not measured, while values for six layers were measured. The limited amount of data, as well as the lower probability of measuring multiple layers, could explain this.
The variation within the data is most probably due to the uncertainties during the graphical analysis. The manual selection of points of interest described above and improper plane corrections are feasible major culprits. Additionally, variation within the z-Piezo calibration could be an error source, however, this seems unlikely, as this would be a systemic cause which would also show in the distance measurements of the single and double plane. As these correspond quite well with the expected values, the Piezo calibration error is negligible. Though the STM is set-up on a vibration-dampening table, large enough tremors during the measurement process which move the measuring tip could also cause problems within the measurement. Further discrepancies could be due to signal loss within the wires of the highly sensitive set-up, or the changing atmospheric conditions during the lab. Some of these artifacts were then repaired during post-processing by using different filters.

## 5 Examination atomic structure

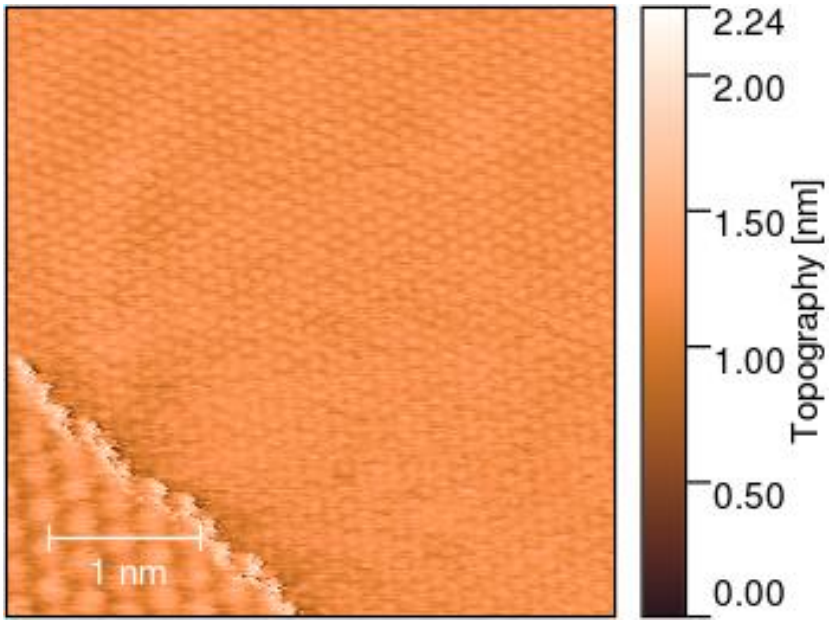


Figure 10: Atomic resolution of graphite obtained via STM-imaging

After not being able to find atomic resolution in the lab, the tutor provided example images. These images were processed with the programm Gwyddion. In figure 10 the edited picture is shown. There is a big step on the left lower corner, which created a lot of noise in the 2FFT. To reduce this the image was cropped as shown in figure 11 and the 2FFT was made.

### 5.1 Fast Fourier transformation

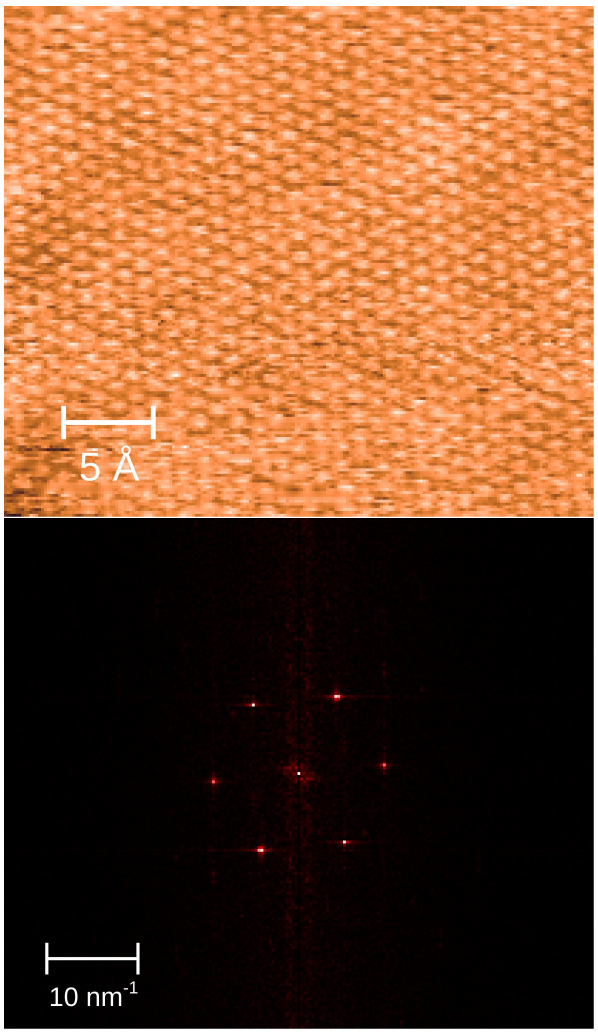


Figure 11: Smaller cut-out of the atomic resolution and it 2FFT

One can clearly see the hexagonal atomic structure in the upper picture and in the reciprocal space in the lower picture on figure 11. The 2FFT should show the first order in the reciprocal space. To determine the real lattice constant a, the wave vector k in the reciprocal space was measured with the length measuring function in Gwyddion. The measuring function was difficult to use as the computer kept having problems with executing Gwyddion. Therefore a systematic error of 0.5 was estimated as listed in table 1

Table 1: Measurements for k

| mesure direction | k vektorlenght in reciprocal space | error |
|---|---|---|
| top left to center | 9,9 | 0,5 |
| middle left to centr | 9,1 | 0,5 |
| bottom left to center | 10,4 | 0,5 |

The formula for the real lattice constant a for a hexagonal lattice is:

$$a = \frac{4\pi}{k\sqrt{3}} \tag{3}$$

The errors for a were calculated using the gaussian method, which leads to the results in table 2

Table 2: Results for k and a with errors

| vectorlength k in reciprocal space | real space lattice constant a in Å |
|---|---|
| 9,9±0,5 | 0,733±0,037 |
| 9,1±0,5 | 0,797±0,044 |
| 10,4±0,5 | 0,698±0,034 |

If we compare this with the theoretical value for the planar distance between closest neighbours d=1,42Å we seem to have found half of that for our a. For the angle between atomic directions, the image in figure 11 was further analysed with the Measure Lattice function as shown in figure 12

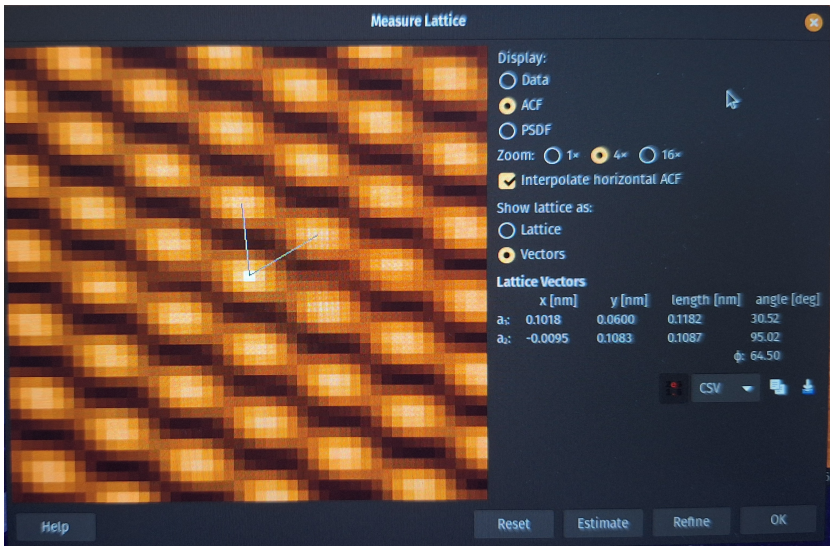


Figure 12: Angle between atomic directions measured with gwyddion

As seen in figure12, the angles between atomic directions equals $\phi$=64,50°. Since it was difficult to correctly adjust the vectors in the program, an error of 3° is considered. The result is $\phi = 64,50° \pm 3,0°$. This is compatible with the expected value for graphene of $\phi$=60°.

# 6 Dependency of the image from different parameters

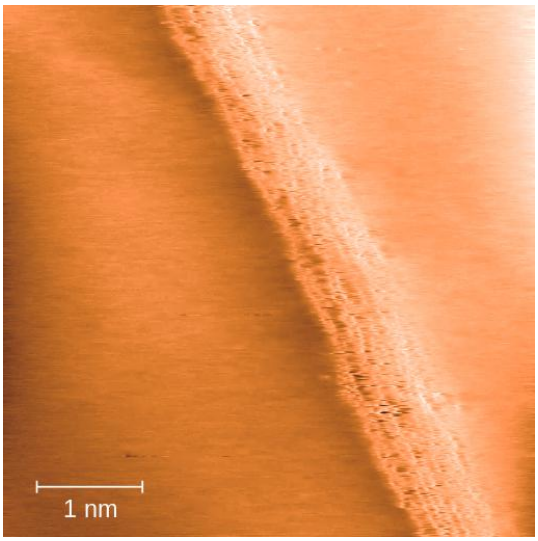


(a) 5nm*5nm

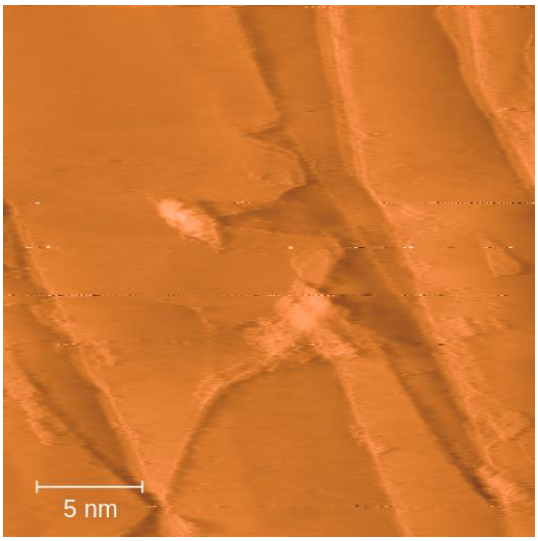


(b) 25nm*25nm

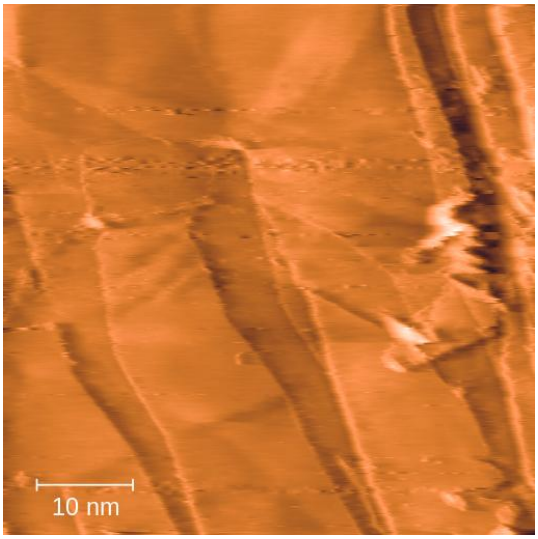


(c) 55nm*55nm

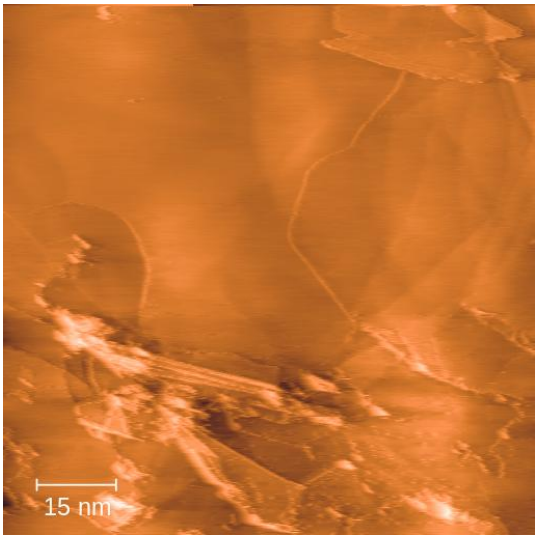


(d) 100nm*100nm

Figure 13: Changing parameters for different image sizes

Table 3: Variing parameters for different images

| image | size in nm*nm | speed in $\frac{lines}{s}$ | bias in mV | set point in mA | proportional gain |
|---|---|---|---|---|---|
| a) | 5*5 | 0,603 | 70 | 5 | 0,126 |
| b) | 25*25 | 0,957 | 70 | 1 | 0,1145 |
| c) | 55*55 | 0,904 | 70 | 1 | 0,086 |
| d) | 100*100 | 0,904 | 70 | 1 | 0,12 |

In general it is difficult to distinguish the impact between the different parameter settings. Since several parameters during one and the same measurement are changed, it is more decisive what the collective change of parameters does, which makes it hard to trace back the effect of a single parameter.
For every measurement, regardless the size of the image, a very slow speed is required to achieve a high quality regarding the resolution. No speed above $1\frac{\text{lines}}{\text{s}}$ is used, the average speed is $0,842\frac{\text{lines}}{\text{s}}$. While the first measurement was taken with the lowest speed, as shown in 3, the following ones were taken with the highest speed possible to minimize the scan time. A change of the bias did not improve the image and thus was not changed at all since the initial setting showed good results.
The set point, which is the setting for the tunneling current $I_t$, was reduced after the first measurement to a lower value, so the distance between the tip and the sample was minimized. This also leads to a higher resolution and although it can also increase the risk of collision between tip and sample, in this case the risk as out of the setting range.
For the proportional gain P, the values in the setting were kept relatively low. Therefore the corrections in z-direction were not as fast and reactive as possible, but the quality of the images seemed to decrease with a higher value. This could be due to a destabilization of the set up, nevertheless the lower values in proportional gain reflect in a slightly smoother or washed out images quality. The integral gain I, which is another correction for the piezo element in z-direction in form of an integral over $I_t$, was changed with the proportional gain since $I = \frac{P}{2}$ applies.
In conclusion, the optimal resolution was achieved for the picture $b$) as shown in 13b. For this image, the chosen settings could provide a high quality image in which, even if a little smoothed out, many details are fully visible. The scan area of $25 * 25$nm seems to be a good compromise when it comes to resolution on atomic scale.

# 7 Summary

This experiment introduced the operation and set-up of a scanning tunneling microscope through exploring the properties of graphite. The height between graphite layers was determined and largely coincided with the expected literature values. Through fast Fourier transformation the real space lattice constant as well as the angle between atomic directions were found. The experimentally identified lattice constant is half of the literature value of $d = 1,42$Å, indicating a systemic error within the analysis. Perhaps the second order for the wave vector was measured, instead of the first. The found angle between atomic directions of $\phi = 64,50° \pm 3,0$ is compatible with the value of $\phi = 60°$ found in literature.
The dependency of the image from different parameter settings could only be analyzed superficially. The most significant impact on the image quality is due to the scan time, so it was increased as much as possible regarding the time limit of the experiment. Since only with a very high scanning time, and thus high quality of the image, the impact of the other parameters became visible, it was difficult to adjust every parameter perfectly. The adjustment for a single picture could take up to half an hour like this, which was not possible within the time frame. Instead, some settings like the bias were kept constant since the quality seemed to be sufficiently good.
The task could be processed more efficiently, if only single parameters were to change to really

observe their impact on the quality of the image.

## References


[1] Introduction to the experiment in english, https://wiki.physik.fu-berlin.de/fp/_media/private:ba10_eng2022.pdf

[2] Spatial structure of solids, https://www.chemie.de/lexikon/FestkÃűrper.html

[3] Scheme of the $sp^2$-hybridization of carbon atoms, https://www.chemistrysteps.com/sp3-sp2-and-sp-hybridization-organic-chemistry/

[4] Hybridization of carbon atoms, https://www.u-helmich.de/che/EF/inhaltsfeld-1/9-Kohlenstoff/seite-9-0-2-Modifikationen.html

[5] Graphite, https://jinsuncarbon.com/graphite-structure/

[6] Spatial structure of graphite, https://allen.in/jee/chemistry/hybridization-of-graphite

[7] Highly oriented pyrolyctic graphite, https://www.sciencedirect.com/topics/engineering/highly-oriented-pyrolytic-graphite

[8] ABAB stacking of graphene layers, https://www.helmholtz-berlin.de/pubbin/news_seite?nid=24109;sprache=de/1000

[9] Fermi-Energy, https://studyflix.de/ingenieurwissenschaften/fermi-energie-1641

[10] BA10-Scanning tunneling microscope, https://wiki.physik.fu-berlin.de/fp/_media/private:ba10_eng2022.pdf

[11] Fourier transformation in STM, https://www.nano.geo.uni-muenchen.de/lectures/MaWi_STM.pdf

[12] Visual representation of Fourier transformation in STM, https://www.sciencedirect.com/science/article/abs/pii/S0008622314011026

[13] Scanning tunneling spectroscopy, https://wiki.physik.fu-berlin.de/fp/_media/private:feenstra_1994_surfsci.pdf

[14] PID Controller explained, https://pidexplained.com/pid-controller-explained/

[15] Block diagram of the STM (by Frank Trixler, Ludwig-Maximilians-Universität München), https://wiki.physik.fu-berlin.de/fp/_media/private:ba10_eng2022.pdf

[16] Schematic of Quantum Tunneling, https://de.wikipedia.org/wiki/Tunneleffekt#/media/Datei:TunnelEffektKling1.svg

[17] Tunneleffekt, Wikipedia, https://de.wikipedia.org/wiki/Tunneleffekt

[18] Piezoelectrizität, Wikipedia, https://de.wikipedia.org/wiki/PiezoelektrizitÃđt

[19] Scanning tunneling microscopy, P. K. Hansma, J. Tersoff, Journal of Applied Physics, 1987, https://wiki.physik.fu-berlin.de/fp/_media/private:hansma_1987_jap.pdf

[20] Gwyddion Program, https://gwyddion.net/